



HAL
open science

Role of MOF surface defects on the microscopic structure of MOF/polymer interfaces: A computational study of the ZIF-8/PIMs systems

Rocio Semino, Naseem A. Ramsahye, Aziz Ghoufi, Guillaume Maurin

► To cite this version:

Rocio Semino, Naseem A. Ramsahye, Aziz Ghoufi, Guillaume Maurin. Role of MOF surface defects on the microscopic structure of MOF/polymer interfaces: A computational study of the ZIF-8/PIMs systems. *Microporous and Mesoporous Materials*, 2017, 254, pp.184-191. 10.1016/j.micromeso.2017.02.031 . hal-01631750

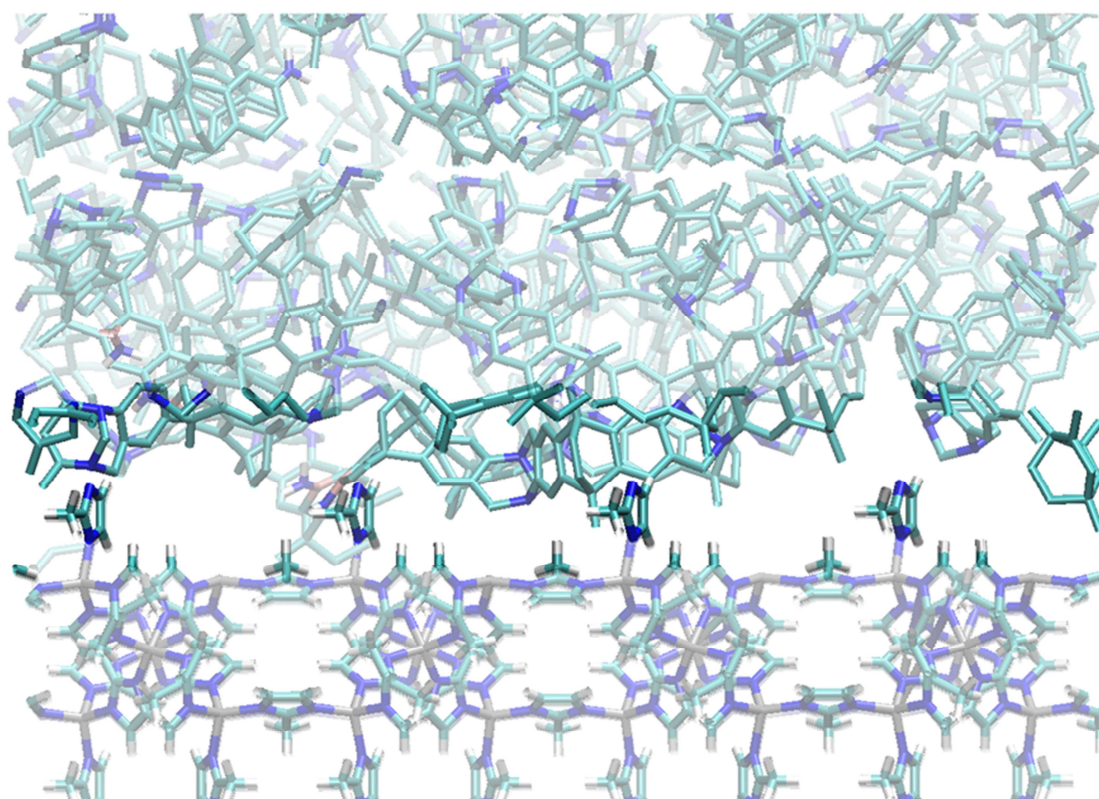
HAL Id: hal-01631750

<https://univ-rennes.hal.science/hal-01631750>

Submitted on 8 Jun 2018

HAL is a multi-disciplinary open access archive for the deposit and dissemination of scientific research documents, whether they are published or not. The documents may come from teaching and research institutions in France or abroad, or from public or private research centers.

L'archive ouverte pluridisciplinaire **HAL**, est destinée au dépôt et à la diffusion de documents scientifiques de niveau recherche, publiés ou non, émanant des établissements d'enseignement et de recherche français ou étrangers, des laboratoires publics ou privés.



ACCEPTED

Role of MOF surface Defects on the microscopic structure of MOF/polymer interfaces: A computation study of the ZIF-8/PIMs systems

Rocio Semino[†], Naseem A. Ramsahye^{†,‡}, Aziz Ghoufi[⊥], Guillaume Maurin^{†*}

[†] Institut Charles Gerhardt Montpellier UMR 5253 CNRS, Université de Montpellier, Place E. Bataillon, 34095 Montpellier Cedex 05, France.

[‡] Institut Charles Gerhardt Montpellier, UMR CNRS 5253 UM2 ENSCM UM1, ENSCM, 8 rue de l'Ecole Normale, 34296 Montpellier Cedex 05, France

[⊥] Institut de Physique de Rennes, IPR, UMR CNRS 6251, 263 Avenue du Général Leclerc, 35042 Rennes, France.

*corresponding author- email : gmaurin@um2.fr

Abstract

The influence of defects at the metal-organic framework (MOF) surface on the microscopic structure of a MOF/polymer composite has been studied by a computational methodology that combines density functional theory calculations with force field-based molecular dynamics simulations. This has been applied to composites formed by ZIF-8 and two different polymers of intrinsic microporosity: PIM-1 and PIM-EA-TB. Analysis of the MOF/polymer interactions, surface coverage, polymer conformation/stiffness and a full characterization of the interfacial voids are provided. We found that, although the nature of the MOF/polymer interactions changes in the presence of defects, the coverage and conformation of the polymer as well as the morphology of the “interfacial microvoids” remain practically unchanged from a microscopic point of view. These results suggest that there is no microscopic evidence that defective MOF surfaces drastically change the geometry of the MOF/polymer interface and the strength of the physisorption-type interactions in play.

Graphical abstract

Keywords

MOF/polymer interface, defects at MOF surfaces, molecular dynamics, density functional theory, mixed-matrix membranes, ZIF-8, PIM-1, PIM-EA-TB

1. Introduction

Metal-organic frameworks are nanoporous crystalline solids composed of metal cations interconnected by organic linkers. These materials have attracted considerable attention due to their potential industrial applications in diverse areas including sensors,[1,2] gas adsorption and separation,[3,4,5,6] and catalysis [7,8,9], among others.[10,11] The presence of defects in MOF crystals is well-documented,[12,13] and they can even be engineered;[14] they can arise from the absence of organic linkers or metal centers (point defects), but extended structural defects can also be found. It is very likely that defects play an important role in the increased reactivity that leads to the chemical instability of MOFs.[15] However, the presence of defects has also been shown to be a key parameter to enhance the MOF's properties in diverse fields including adsorption,[16,17,18,19] catalysis,[20,21,22,23] as well as applications relying on electronic[24,25] and mechanical properties.[26,27]

MOF/polymer composites have been widely studied due to their applications in membranes for gas separation.[28,29] The objective is to combine the processability of polymers with the sieving effect of MOFs. In addition, if a polymer with high permeability is selected, such as the polymers of intrinsic microporosity (PIMs)[30,31], the resulting composite membrane could potentially exhibit both high permeability and high selectivity. However, the synthesis of MOF/polymer membranes with good

morphologies and performances is challenging. In a recent review, several strategies were presented that could lead to an improvement in the design of these membranes.[32] Among these strategies was the tailoring of MOF surfaces in order to modify surface properties and improve adhesion with the polymers. Some examples have proven that the decoration of the MOF surface with organic molecules could be beneficial for some practical applications, such as gas separation.[33,34] Another way to achieve this improvement would be to introduce “defects” at the MOF surface. In fact, surfaces are likely to have a relatively significant concentration of “defects”, and it is important to understand how their presence affects the structure and physicochemical properties of the surface with respect to those of the “defect-free” case. Therefore, a microscopic study comparing influence of defects at the MOF external surface on the microscopic properties of the MOF/polymer interface to those of the “defect-free” case is of great interest.

Recently, we have developed a computational methodology to model the MOF/polymer interfaces, integrating high-level quantum calculations with force field-based molecular dynamics simulations, and applied it to analyze the microscopic properties of the ZIF-8[35]/PIM-1 (scheme in Fig. 1c) [30] interface as a model system.[36] This computational tool has been further used to study a new composite of the same MOF, with a different polymer, namely the ZIF-8/PIM-EA-TB (scheme in Fig. 1d) [31] interface.[37] We have evidenced that the ZIF-8/PIM-1 composite exhibits favorable attractive interactions between the MOF and the polymer, that act as anchoring points.[36] In contrast, the ZIF-8/PIM-EA-TB composite shows no preferential interactions, but instead exhibits a homogeneous set of interactions that leads to a better surface coverage.[37] Both composites have been found to have “microvoids” at the interface, with diameters that can go up to 13 Å and 11 Å respectively. These “microvoids” could provide a microscopic-level explanation of a sub-optimal compatibility between the MOF/polymer pairs that has been revealed.[37] The objective of this paper is to predict whether the introduction of defects at the MOF surface would drastically change the microscopic structure of the

MOF/polymer interface and the interactions in play. In a previous contribution [36] the model ZIF-8 surface slab was “defect-free” (see Fig. 1a). Here, we introduce a “defect-containing” ZIF-8 surface slab, which consists of under-coordinated metal atoms and deprotonated organic linkers (see Fig. 1b), we present a full characterization of the resulting interfaces of the MOF/polymer composites with both PIM-1 and PIM-EA-TB, and the corresponding results are compared with those of the “defects-free” system.

This paper is organized as follows. We first discuss the computational methodology that we have applied for the construction of the defective MOF surface/polymer interface, (section 2) followed by a discussion of the main results obtained for the characterization of the composite in section 3. Finally, we present the concluding remarks in section 4.

2. Methodology

The model interfaces have been constructed by applying the multiscale methodology that we have previously developed and applied to the ZIF-8/PIM-1 and ZIF-8/PIM-EA-TB “defect-free” (D0) interfaces.[36,37] Basically, the methodology involves density functional theory (DFT) calculations for optimization of the MOF surface model, which is then coupled with a polymer to create an initial composite model. Force-field Molecular Dynamics (MD) simulations are then applied to refine and optimize this model, and subsequently calculate the required properties for a full analysis.

The ZIF-8 “defect-containing” surface slab (D1) was generated from the most stable [011] “defect-free” surface we previously reported. Here the under-coordinated atoms, which were initially terminated considering the dissociative adsorption of water molecules in the defect-free case,[36] were left uncapped. As a result, while the D0 surface consists of two types of terminations: OH groups and imidazole moieties bonded to the Zn external atoms, in an alternate fashion (see Fig. 1a), the D1 surface

contains uncapped Zn atoms and imidazole moieties (see Fig. 1b). For the subsequent MD simulations, the MOF surface model was kept rigid, the flexibility of the surface for this systems has been shown to have a negligible effect on the interfacial properties.[36] All atoms of ZIF-8 were treated as charged Lennard-Jones (LJ) sites. A full list of the LJ parameters and partial charges we have used can be found in the Supporting Information.

The PIM-1 and PIM-EA-TB polymers (see Fig. 1c and 1d respectively) were constructed by combining the *Polymatic* code[38] and LAMMPS software,[39] considering boxes of 50 Å x 50 Å x 150 Å. The bonded parameters were taken from the GAFF force field.[40] The non-bonded interactions were modeled as a sum of site to site 12-6 Lennard-Jones (LJ) potentials and Coulombic interactions. The LJ parameters were taken from TraPPE force field,[41] and the crossed potential LJ parameters were computed by using the Lorentz-Berthelot mixing rules.[42] The ESP partial charges for PIM-EA-TB and PIM-1 were computed by DFT calculations. Further details on the polymer models can be found in our previous publications.[36,37] The full list of force-field parameters is available in the Supporting Information.

After generating the polymer models, two empty boxes were added in the z direction, resulting in boxes of 50 Å x 50 Å x 400 Å. The polymers were then equilibrated following the 21-steps MD equilibration scheme proposed by Hoffman *et al*[43] (ensembles and thermodynamic conditions are shown in Table S4, polymer equilibration). The coordinates of the polymers were unwrapped in the z direction, and then the ZIF-8 “defect-containing” surface was added, by putting the two simulation boxes together in the z direction. Again, a 21-steps MD equilibration was performed, but this time, the constant pressure simulations were carried out so that the cell could only change its volume by variations of its length in the z direction (NP_nT ensemble instead of NPT ensemble, see Table S4, interface generation). Here again, the MOF/polymer interactions were treated as the sum of a LJ term and a Coulombic contribution, the crossed LJ potential parameters being computed by using the Lorentz-Berthelot mixing

rules. Statistical data were collected for 10 MD simulations in the NVT ensemble for each different system, with each simulation lasting 10 ns. The 10 independent MD initial configurations for these runs were generated as follows: the polymer as obtained from *Polymatic*[38] was subjected to 10 different simulated annealing protocols, which consisted of 10 consecutive heating/cooling cycles in the NVT ensemble, and the high and low temperatures as well as the duration of the cycles were varied. This procedure resulted in 10 independent polymer configurations, which were subsequently equilibrated first without and then in the presence of the MOF surface slab (21 steps schemes previously described). All MD simulations were performed using a cutoff of 15 Å for the vdW interactions, while the Ewald summation was used for the electrostatic interactions. The Berendsen thermostat and barostat [44] were used in the NVT and NPT/NP_nT simulations respectively, with relaxation times of 0.1 ps for the thermostat and 0.5 ps for the barostat. The interface simulations were performed by using the DLPOLY classic software,[45] which was modified in order to allow for the use of NP_nT ensemble.

3. Results & Discussion

In order to characterize the interactions between the polymers and the ZIF-8 D1 surface, we have computed radial distribution functions (RDFs) for different MOF/polymer atom pairs. The data are summarized in Figs. 2 and 3 for the ZIF-8(D1)/PIM-1 and ZIF-8(D1)/PIM-EA-TB interfaces respectively.

PIM-1 strongly interacts with the under-coordinated Zn atoms at the ZIF-8(D1) surface through its CN group, with an average distance of 1.9 Å (see Fig. 2, bottom left panel). The rest of the MOF/polymer pairs show much weaker interactions associated with characteristic distances greater than 5.0 Å. This behavior differs to that previously observed for the “defect-free” interface where the CN group of PIM-1 has been found to interact with the NH groups of the ZIF-8 imidazole moiety, with a characteristic distance of 2.6 Å.[36] Regarding PIM-EA-TB, multiple interactions can be found as in the “defect-

free” surface case, however the atoms involved are not the same. In the “defect-containing” interface, several sites, including the amino groups of the polymer interact with the hydrogens of ZIF-8 (labeled as H1 and H4 in the force field, see Supporting Information), with average distances of around 3 Å (see Fig. 3). This range of distance is the same as that measured for the ZIF-8(D0)/PIM-EA-TB interface. [37] However, in that case, the different polymer sites interact with the NH groups in the imidazole moiety, which is absent in the “defect-containing” model surface.

As a next step, we have studied the polymer coverage at the interfaces. Fig. 4 shows the density of the MOF and the polymer atoms for ZIF-8(D1)/PIM-1 and ZIF-8(D1)/PIM-EA-TB as a function of the z -coordinate, which corresponds to the direction perpendicular to the MOF surface plane. The profiles are similar to those obtained for the ZIF-8(D0)/PIM-1 and the ZIF-8(D0)/PIM-EA-TB interfaces. In all cases, the density of polymer atoms oscillates around a constant value. The density then decreases linearly as it approaches polymer/ZIF-8 interface until reaching zero at the MOF surface. Thus, two distinct regions can be identified: the interfacial region, **region A**, and a more “bulk-like” region, **region B**. The z -length of **region A** can be used as a parameter to compare the surface coverage by the polymers. We define this parameter as the distance between the most external Zn atoms in the MOF and the z value from where the polymer density starts fluctuating around a constant value. The average values for the 10 MD runs are (12 ± 4) Å and (9 ± 2) Å for the ZIF-8(D1)/PIM-1 and ZIF-8(D1)/PIM-EA-TB composites respectively, where the error bar was considered as the standard deviation of the values. These values are similar to those obtained for the analogue “defect-free” composites, (13 ± 2) Å and (9 ± 1) Å. Snapshots of the two “defect-containing” interfaces are shown in Fig.5, **regions A** and **B** are labeled and the typical MOF/polymer interactions are shown.

Furthermore, we have studied the free volume distribution at the interface. To this end, two different methodologies were employed. On the one hand, the $v_connect$ method,[46] and on the other, that developed by Bhattacharya *et al.*[47] Following the first approach, we superimposed a three-

dimensional grid with bin sizes of 0.7 Å to the different interfaces, and classified the grid cubes as “empty” or “full”. Then, a probe molecule, with the size of a positronium particle or a nitrogen molecule (diameter 2.2 Å and 3.64 Å respectively), was used to sample the empty cubes. Finally, the voids are classified by their volume, and by the diameter they would have if they were spherical. As its name indicates, this methodology is supposed to account for the connectivity of the voids, provided the bin size is sufficiently small. The second methodology samples the voids by introducing a sphere and increasing its diameter in a given position of space, up to the point where it overlaps with the interface atoms.

Figs. S2 and S3 depict histograms for the void distribution probed by using these methodologies for **regions A** and **B** of the ZIF-8(D1)/PIM-1 and ZIF-8(D1)/PIM-EA-TB interfaces respectively. The top and middle panels correspond to the $v_connect$ results. The top panels show the number of voids as a function of their equivalent spherical diameter. Smaller voids are generally more abundant than larger ones. However, the larger ones represent a larger fraction of the total free volume, as illustrated by the middle panels. The graphs in the lower panels show similar results to those obtained by the $v_connect$ methodology, proving thus that there is low interconnectivity between the different voids.

Table 1 shows the values for the maximum equivalent spherical diameters for the “defect-free” and “defect-containing” interfaces (**regions A** and **B**) as well as for the pure polymers. The maximum equivalent spherical diameter is similar for **regions A** and **B** in both cases: (13 ± 2) Å versus (10 ± 1) Å for the PIM-1 composite and (12 ± 1) Å vs (10 ± 3) Å for the PIM-EA-TB composite. Comparing these results with the “defect-free” interfaces, the “interfacial microvoids” (**region A**) are similar as well, with the equivalent spherical diameter being (13 ± 1) Å for ZIF-8(D0)/PIM-1,[36] and (11 ± 1) Å for ZIF-8(D0)/PIM-EA-TB.[37]

For both the ZIF-8(D1)/PIM-1 and the ZIF-8(D1)/PIM-EA-TB interfaces, **region B** shows only microvoids, and not highly interconnected mesoscopic voids as in the case of pure polymers, as reported

in previous studies by using the same methodology: the bulk PIM-1 has been found to exhibit voids of up to 34 Å,[48] while PIM-EA-TB shows slightly smaller mesopores of 32 Å in diameter, as probed by a positronium particle.[49] This suggests that the influence of the MOF surface extends even to **region B**, similarly to what was found for the “defect-free” interfaces.[36,37] The size of the microvoids in **region B** is similar for both PIM-EA-TB composites: (10 ± 3) Å and (10 ± 1) Å, and for PIM-1 composites as well: (10 ± 1) Å versus (8 ± 1) Å, for the D1 and D0 surfaces respectively.

To obtain further insight on the shape of the voids, we computed their associated eccentricity:

$$e = \sqrt{1 - \frac{b^2}{a^2}}$$

where b and a are the minor and major axis of the ellipse. For a perfect sphere, $e = 0$, while for a very elongated ellipse, its value approaches 1. The distribution of the eccentricity values for **region A**, “interfacial microvoids”, for the different interfaces is plotted in Fig. 6. Comparing the “defect-free” and “defect-containing” interfaces, the PIM-1 composites eccentricity profiles closely resemble (see top panels), while for the PIM-EA-TB, the proportion of more spherical-like voids increases to the detriment of the more elongated elliptical ones when considering the “defect-containing” ZIF-8 surface. The tendency in the relative proportion of spherical-like voids versus the elliptical ones for the different polymers changes with the considered surface is that more spherical-like voids are found for PIM-1 than for PIM-EA-TB in the “defect-free” case, while the reverse is true for the “defect-containing” surfaces. The $v_{connect}$ methodology also allows for an estimation of the free volume fraction of the interface, by computing the percentage of free cubes with respect to the total number of cubes in the three-dimensional grid. The estimated free volume fraction is 0.25 ± 0.01 for ZIF-8(D0)/PIM-1 and ZIF-8(D1)/PIM-1 composites, and 0.23 ± 0.01 and 0.24 ± 0.02 for ZIF-8(D0)/PIM-EA-TB and ZIF-8(D1)/PIM-EA-TB interfaces respectively. The error was taken as the standard deviation for the 10 MD

runs in each case. These values show that although the systems are different in terms of their microscopic characteristics (interactions and voids distributions), the total available free volume is similar for all the composites. In addition, these values are comparable to those for the bulk polymers, namely 0.24-0.26 for PIM-1 and 0.27-0.28 for PIM-EA-TB.[49]

Finally, we have analyzed the conformation of the polymer at the interface by computing the distribution of some key dihedral angles in the polymer phases for the “defect-containing” and “non-defect-containing” cases. The contorted backbone and high rigidity are distinctive features that create permanent porosity with unusually high BET area in the PIMs. It is thus interesting to study the stiffness of the polymer at the interface, along with its porosity. Fig. 7 shows two dihedral angles distributions for PIM-1. The plot includes the data presented in our previous contribution for the D0 interface in black,[36] and the new data in red. The profiles are almost identical, which means that despite changing the nature of the interactions, the “anchoring points” scheme gives a very similar polymer conformation. As mentioned in our previous contribution,[36] when comparing these results with the pure polymer ones,[48] the conformation is found to change drastically. The degrees of freedom are reduced in the presence of the surface, and the interfacial polymer is even more rigid than the bulk one.

Fig. 8 shows the distribution of a torsional angle involving the bicyclic TB units in PIM-EA-TB, for the D0 and D1 interfaces. As for PIM-1, while the distributions look very similar, they are quite different from that of the bulk polymer.[49] The bulk polymer showed two peaks: one high-intensity peak with a maximum of 95° , and a low-intensity one at -110° . Here, the high-intensity peak is still present, but shifted in 25° : the maximum is around 119° and 124° for the polymer at ZIF-8(D0) and ZIF-8(D1) interfaces respectively. The low-intensity peak is replaced for a more uniform low-intensity region between -180° and 20° . This means that PIM-EA-TB can adopt certain angles that were prohibited in the presence of the MOF, although with a low probability.

4. Conclusion

We have modeled two “defect-containing” ZIF-8/PIMs composites at the atomistic level by applying a methodology combining DFT calculations and force field-based MD simulations. Our results are compared with those of the “defect-free” interfaces. The interactions between the MOF and the polymer depend on the nature of MOF surface. However, the general picture remains the same for both PIMs. PIM-1 interacts through its cyano- function in both cases, with the NH termination at the imidazole moiety at the “defect-free”, and with the bare Zn at the “defects-containing” ZIF-8 surface. This leads to a series of “anchoring points” at the surface regardless the presence/absence of defects. For the PIM-EA-TB interfaces, many polymer atoms are involved in the interactions, both for the “defect-free” and “defect-containing” ZIF-8. In the former, the interactions are mainly with the -NH group of the imidazole moiety, while in the latter, they take place with the H atoms that are bonded to the C atoms on the imidazolate linkers.

As for the “defect-free” cases, “interfacial microvoids” were found, and the systems can be divided in two distinct regions: **region A**, where the polymer density drops linearly with the distance to the MOF surface, and **region B**, a more “bulk-like” polymer. The coverage of the surface by the polymer and the size of the voids are similar between the “defect-free” and “defect-containing” cases. **Region B** polymers still differ from the corresponding bulk polymers, as was previously found for the “defect-free” interfaces, so that the influence of the surface in the polymer configuration extends up to more than 15 Å. The probability distribution of the shape of the voids is almost unchanged when comparing ZIF-8(D0)/PIM-1 and ZIF-8(D1)/PIM-EA-TB, but there is an increase of spherical-like voids in detriment of the elliptical ones in the “defect-containing” case for PIM-EA-TB composites. The total free volume fraction is similar in all cases, and comparable to that of the pure polymers.

The conformation of the PIMs at the interface changes with respect to their bulk conformations. Nevertheless, the presence of defects at the surface does not seem to significantly change the polymer

conformation. PIM-1 seems to become more rigid in the presence of the interfaces, while PIM-EA-TB has a low probability of adopting certain torsion angles values that were not seen in the bulk.

Overall, the plausible presence of “defects” at the MOF surface seems to induce only minor changes on the characteristics of the interface at the microscopic scale. Indeed, there are no microscopic features to support that the presence of defects at the MOF surface would drastically affect the geometry of the MOF/polymer and the interactions in play. This suggests that the microscopic structure of the MOF/polymer interface is mainly dictated by properties such as geometry and flexibility, while the chemical interactions only play a minor role. A continuation of this work will be to consider the study of these composites at the mesoscopic scale.

Acknowledgements

The research leading to these results has received funding from the European Community Seventh Program (FP7/2007-2013) under grant agreement n° 608490 (project M⁴CO₂). G.M. thanks Institut Universitaire de France for its support.

References

- [1] L. E. Kreno, K. Leong, O. K. Farha, M. Allendorf, R. P. Van Duyne, J. T. Hupp, *Chem. Rev.* 112 (2012) 1105-1125.
- [2] D. Ma, B. Li, X. Zhou, Q. Zhou, K. Liu, G. Zeng, G. Li, Z. Shi, S. Feng, *Chem. Commun.* 49 (2013) 8964-8966.
- [3] J.-R. Li, R. J. Kuppler, H.-C. Zhou, *Chem. Soc. Rev.* 38 (2009) 1477-1504.

- [4] L. Hamon, P. L. Llewellyn, T. Devic, A. Ghoufi, G. Clet, V. Guillerm, G. D. Pirngruber, G. Maurin, C. Serre, G. Driver, W. van Beek, E. Jolimaître, A. Vimont, M. Daturi, G. Férey, *J. Am. Chem. Soc.* 131 (2009) 17490-17499.
- [5] H. Bux, C. Chmelik, R. Krishna, J. Caro, *J. Membr. Sci.* 369 (2011) 284-289.
- [6] B. R. Pimentel, A. Parulkar, E. K. Zhou, N. A. Brunelli, R. P. Lively, *ChemSusChem* 7 (2014) 3202-3240.
- [7] P. García-García, M. Müller, A. Corma, *Chem. Sci.* 5 (2014) 2979-3007.
- [8] J. Lee, O. K. Farha, J. Roberts, K. A. Scheidt, S. T. Nguyen, J. T. Hupp, *Chem. Soc. Rev.* 38 (2009) 1450-1459.
- [9] L. Ma, C. Abney, W. Lin, *Chem. Soc. Rev.* 38 (2009), 1248-1256.
- [10] A. U. Czaja, N. Trukhan, U. Müller, *Chem. Soc. Rev.* 38 (2009) 1284-1293.
- [11] O. Shekhah, J. Liu, R. A. Fischer, Ch. Wöll, *Chem. Soc. Rev.* 40 (2011) 1081-1106.
- [12] P. S. Petkov, G. N. Vayssilov, J. Liu, O. Shekhah, Y. Wang, C. Wöll, T. Heine, *Chem. Phys. Chem.* 13 (2012) 2025-2029.
- [13] D. S. Sholl, R. P. Lively, *J. Phys. Chem. Lett.* 6 (2015) 3437-3444.
- [14] Z. Fang, B. Bueken, D. E. De Vos, R. A. Fischer, *Angew. Chem. Int. Ed.* 54 (2015) 7234-7254.
- [15] N. C. Burtch, H. Jasuja, K. S. Walton, *Chem. Rev.* 114 (2014) 10575-10612.
- [16] H. Wu, Y. S. Chua, V. Krungleviciute, M. Tyagi, P. Chen, T. Yildirim, W. Zhou, *J. Am. Chem. Soc.* 135 (2013) 10525-10532.
- [17] P. Ghosh, Y. J. Colón, R. Q. Snurr, *Chem. Commun.* 50 (2014) 11329-11331.
- [18] K. M. Choi, H. J. Jeon, J. K. Kang, O. M. Yaghi, *J. Am. Chem. Soc.* 133 (2011) 11920-11923.
- [19] C. S. Tsao, M.-S. Yu, C.-Y. Wang, P.-Y. Liao, H.-L. Chen, U.-S. Jeng, Y.-R. Tzeng, T.-Y. Chung, H.-C. Wu, *J. Am. Chem. Soc.* 131 (2009) 1404-1406.

- [20] F. Vermoortele, M. Vandichel, B. Van de Voorde, R. Ameloot, M. Waroquier, V. Van Speybroeck, D. E. De Vos, *Angew. Chem. Int. Ed.* 51 (2012) 4887–4890.
- [21] T.-H. Park, A. J. Hickman, K. Koh, S. Martin, A. G. Wong-Foy, M. S. Sanford, A. J. Matzger, *J. Am. Chem. Soc.* 133 (2011) 20138–20141.
- [22] J. Canivet, M. Vandichel, D. Farrusseng, *Dalton Trans.* 45 (2016) 4090–4099.
- [23] F. X. Llabres i Xamena, F. G. Cirujano, A. Corma, *Microporous Mesoporous Mater.* 157 (2012) 112–117.
- [24] Z. Fang, J. P. Dürholt, M. Kauer, W. Zhang, C. Lochenie, B. Jee, B. Albada, N. Metzler-Nolte, A. Pöpl, B. Weber, M. Muhler, Y. Wang, R. Schmid, R. A. Fischer, *J. Am. Chem. Soc.* 136 (2014) 9627–9636.
- [25] L. Shen, S.-W. Yang, S. Xiang, T. Liu, B. Zhao, M.-F. Ng, J. Göettlicher, J. Yi, S. Li, L. Wang, J. Ding, B. Chen, S.-H. Wei, Y. P. Feng, *J. Am. Chem. Soc.* 134 (2012) 17286–17290.
- [26] M. J. Cliffe, W. Wan, X. Zou, P. A. Chater, A. K. Kleppe, M. G. Tucker, H. Wilhelm, N. P. Funnell, F.-X. Coudert, A. L. Goodwin, *Nat. Commun.* 5 (2014) 4176.
- [27] S. M. J. Rogge, J. Wieme, L. Vanduyfhuys, S. Vandenbrande, G. Maurin, T. Verstraelen, M. Waroquier, V. Van Speybroeck, *Chem. Mater.* 28 (2016) 5721–5732.
- [28] Q. Song, S. K. Nataraj, M. V. Roussanova, J. C. Tan, D. J. Hughes, W. Li, P. Bourgoïn, M. A. Alam, A. K. Cheetham, S. A. Al-Muhtaseb, E. Sivaniah, *Energy Environ. Sci.* 5 (2012) 8359–8369.
- [29] B. Seoane, J. Coronas, I. Gascon, M. Etxebarria Benavides, O. Karvan, J. Caro, F. Kapteijn, J. Gascon, *Chem. Soc. Rev.* 44 (2015) 2421–2454.
- [30] P. M. Budd, E. S. Elabas, B. S. Ghanem, S. Makhseed, N. B. McKeown, K. J. Msayib, C. E. Tattershall, D. Wang, *Adv. Mater.* 16 (2004) 456–459.
- [31] M. Carta, R. Malpass-Evans, M. Croad, Y. Rogan, J. C. Jansen, P. Bernardo, F. Bazzarelli, N. B. McKeown, *Science* 339 (2013) 303–307.

- [32] Y. Zhang, X. Feng, S. Yuan, J. Zhou, B. Wang, *Inorg. Chem. Front.* 3 (2016) 896-909.
- [33] M. W. Anjum, F. Vermoortele, A. L. Khan, B. Bueken, D. E. De Vos, I. F. Vankelecom, *ACS Appl. Mater. Interfaces* 7 (2015) 25193-25201.
- [34] S. R. Venna, M. Lartey, T. Li, A. Spore, S. Kumar, H. B. Nulwala, D. R. Luebke, N. L. Rosi, E. Albenze, *J. Mater. Chem. A* 3 (2015) 5014-5022.
- [35] K. S. Park, Z. Ni, A. P. Côté, J. Y. Choi, R. Huang, F. J. Uribe-Romo, H. K. Chae, M. O'Keeffe, O. M. Yaghi, *Proc. Natl. Acad. Sci. U. S. A.* 103 (2006) 10186-10191.
- [36] R. Semino, N. A. Ramsahye, A. Ghoufi, G. Maurin, *ACS Appl. Mater. Interfaces* 8 (2016) 809-819.
- [37] M. Benzaqui, R. Semino, N. Menguy, F. Carn, T. Kundu, J. M. Guigner, N. B. McKeown, K. J. Msayib, M. Carta, R. Malpass-Evans, C. Le Guillouzer, G. Clet, N. A. Ramsahye, C. Serre, G. Maurin, N. Steunou, *ACS Appl. Mater. Interfaces* 8 (2016) 27311-27321.
- [38] L. J. Abbott, K. E. Hart, C. M. Colina, *Theor. Chem. Acc.* 132 (2013) 1334.
- [39] Plimpton, S. J. *Comput. Phys.* 117 (1995) 1-19.
- [40] J. Wang, R. M. Wolf, J. W. Caldwell, P. A. Kollman, D. A. Case, *J. Comput. Chem.* 25 (2004) 1157-1174.
- [41] B. L. Eggimann, A. J. Sunnarborg, H. D. Stern, A. P. Bliss, J. I. Siepmann, *Mol. Simul.* 40 (2014) 101-105.
- [42] M. P. Allen, D. J. Tildesley, *Computer Simulation of Liquids*, Oxford Science Publications, Oxford, 1989.
- [43] D. Hofmann, L. Fritz, J. Ulbrich, C. Schepers, M. Böhning, *Macromol. Theory Simul.* 9 (2000) 293-327.
- [44] H. J. C. Berendsen, J. P. M. Postma, W. F. van Gunsteren, A. DiNola, J. R. Haak, *J. Chem. Phys.* 81 (1984) 3684-3690.

- [45] I. T. Todorov, W. Smith, K. Trachenko, M. T. Dove, *J. Mater. Chem.* 16 (2006) 1911-1918.
- [46] D. Hofmann, M. Heuchel, Y. Yampolskii, V. Khotimskii, V. Shantarovich, *Macromolecules* 35 (2002) 2129-2140.
- [47] S. Bhattacharya, K. E. Gubbins, *Langmuir* 22 (2006) 7726-7731.
- [48] M. Heuchel, D. Fritsch, P. M. Budd, N. B. McKeown, D. Hofmann, *J. Membr. Sci.* 318 (2008) 84-99.
- [49] E. Tocci, L. De Lorenzo, P. Bernardo, G. Clarizia, F. Bazzarelli, N. B. McKeown, M. Carta, R. Malpass-Evans, K. Friess, K. Pilnáček, M. Lanč, Y. P. Yampolskii, L. Strarannikova, V. Shantarovich, M. Mauri, J. C. Jansen, *Macromolecules* 47 (2014) 7900-7916.

Table 1. Equivalent spherical diameters (\AA) of the voids for the “defect-free” and “defect-containing” interfaces and for the bulk polymers, obtained by the $v_connect$ method.

Compound	Region A	Region B
ZIF-8(D1)/PIM-1	$(13\pm 2)^1$	$(10\pm 1)^1$
ZIF-8(D0)/PIM-1	$(13\pm 1)^{2,3}$	$(8\pm 1)^{2,3}$
Bulk PIM-1		34^4
ZIF-8(D1)/PIM-EA-TB	$(12\pm 1)^1$	$(10\pm 3)^1$
ZIF-8(D0)/PIM-EA-TB	$(11\pm 1)^3$	$(10\pm 1)^3$
Bulk PIM-EA-TB		32^5

1-This work, 2-Ref. [36], 3-Ref. [37], 4-Ref. [48], 5-Ref. [49]

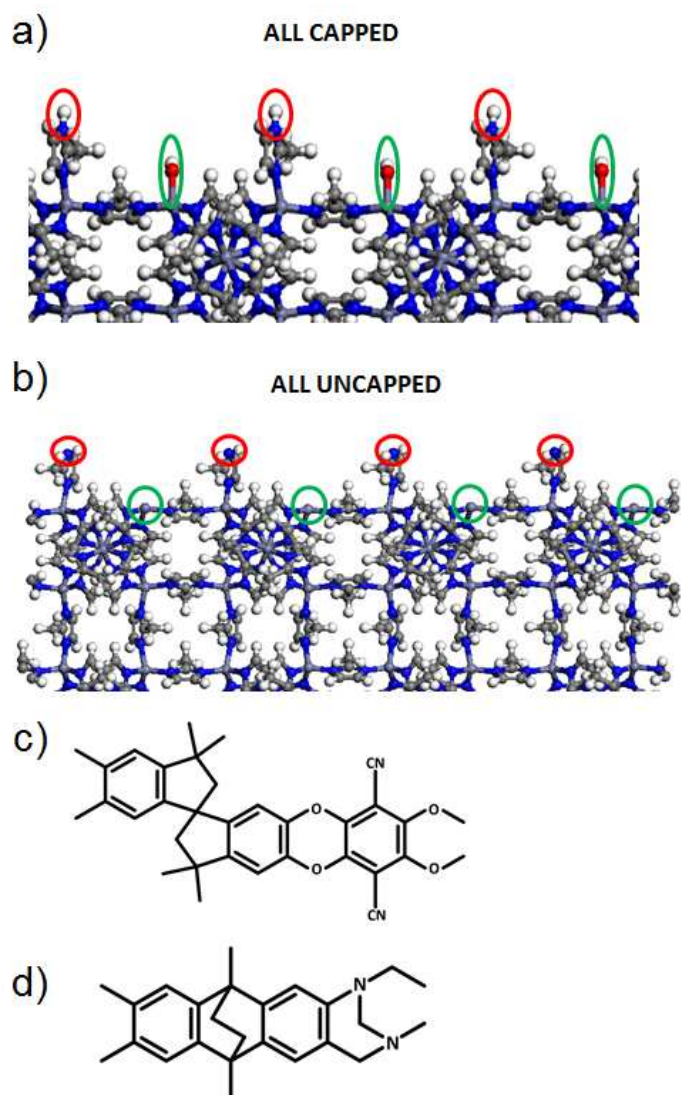


Fig.1. Schemes of model ZIF-8 surfaces: (a) “defect free” surface, (b) “defect-containing” surface labeled as D0 and D1 respectively. The red circles highlight the N terminal imidazole atoms, which are terminated by an H in the “defect-free” surface, and left under-coordinated in the “defect-containing” surface. The green circles indicate Zn atoms which are terminated by an OH group in the “defect-free” surface and left under-coordinated in the “defect-containing” one. Schemes of PIMs: (c) PIM-1 and (d) PIM-EA-TB.

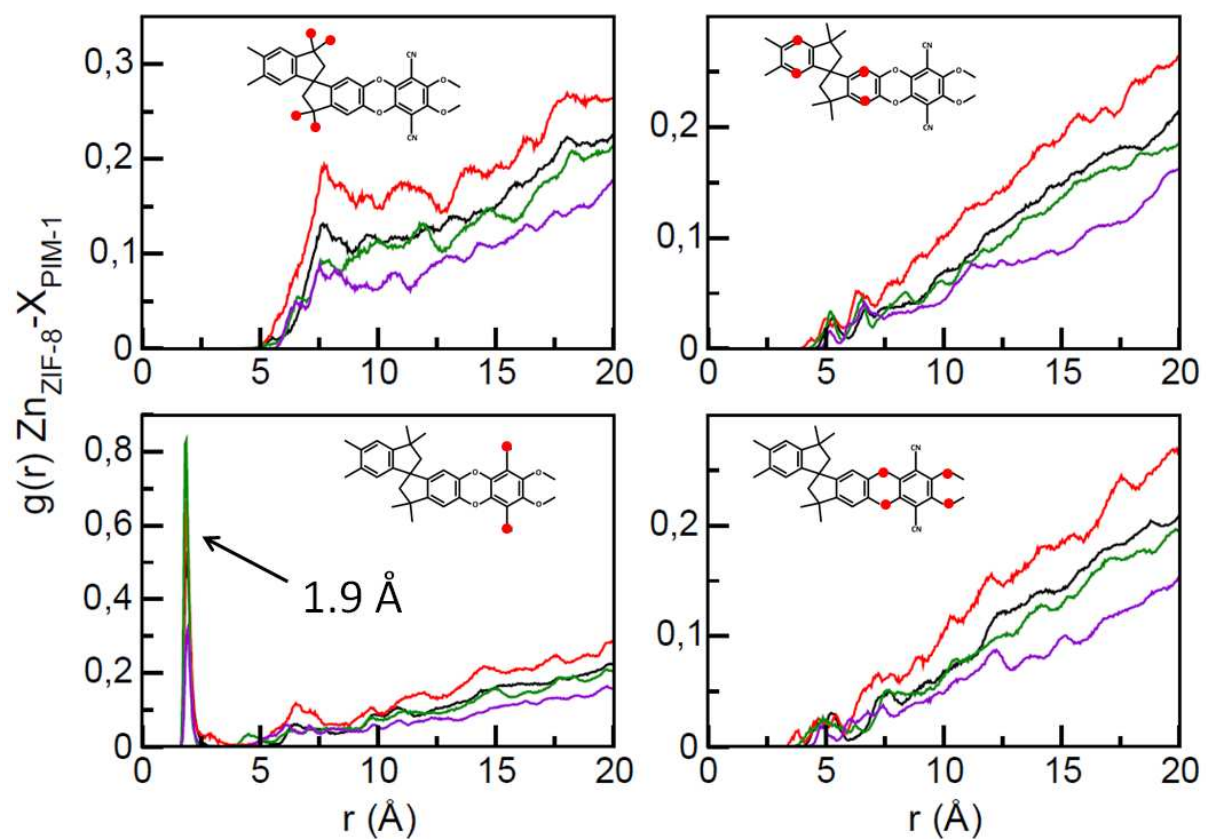


Fig. 2. Radial distribution functions for the ZIF-8(D1)/PIM-1 interface model, for the pairs $(\text{Zn})_{\text{ZIF-8}} \dots \text{X}_{\text{PIM-1}}$. The involved polymer sites are indicated in the schemes in red. Results obtained from four different MD runs.

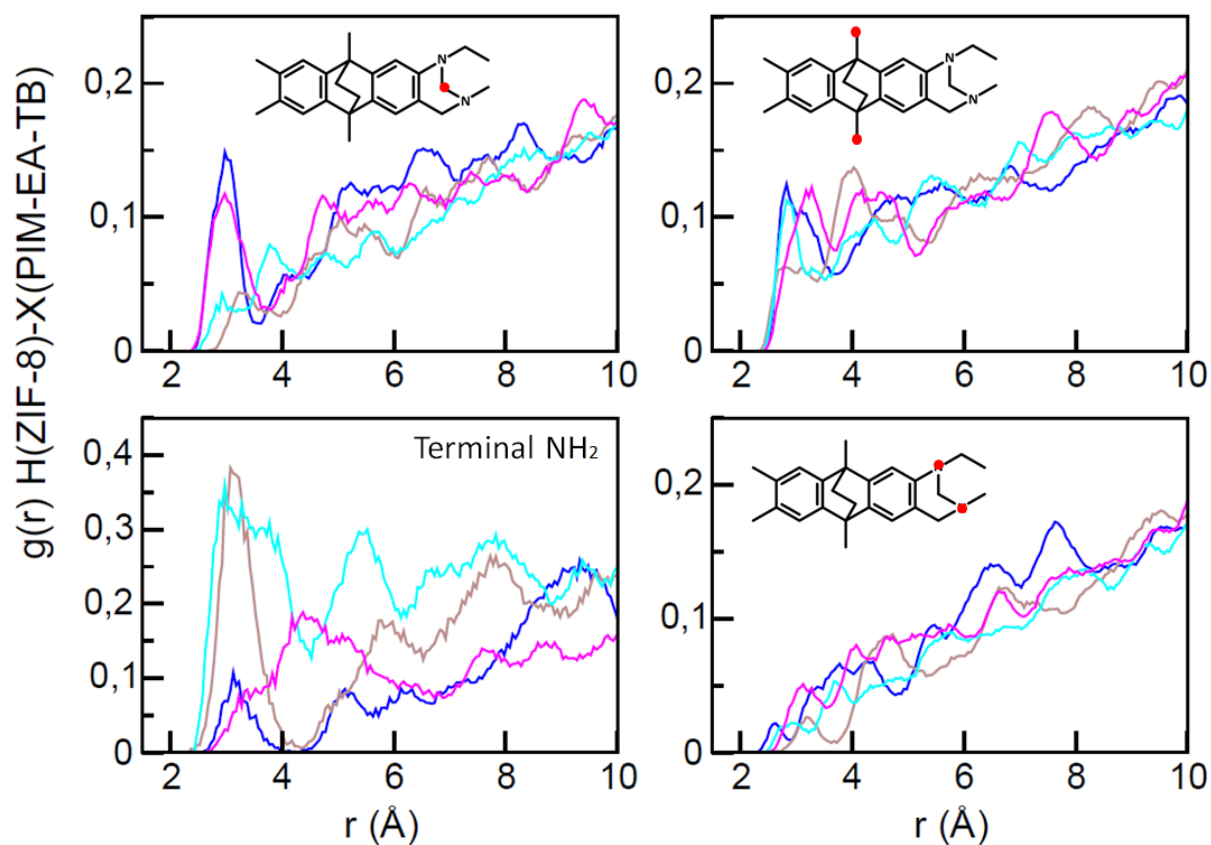


Fig. 3. Radial distribution functions for the ZIF-8(D1)/PIM-EA-TB interface model, for the pairs $(H)_{\text{ZIF-8}} \dots X_{\text{PIM-EA-TB}}$. The involved polymer sites are indicated in the schemes in red. Results obtained from four different MD runs.

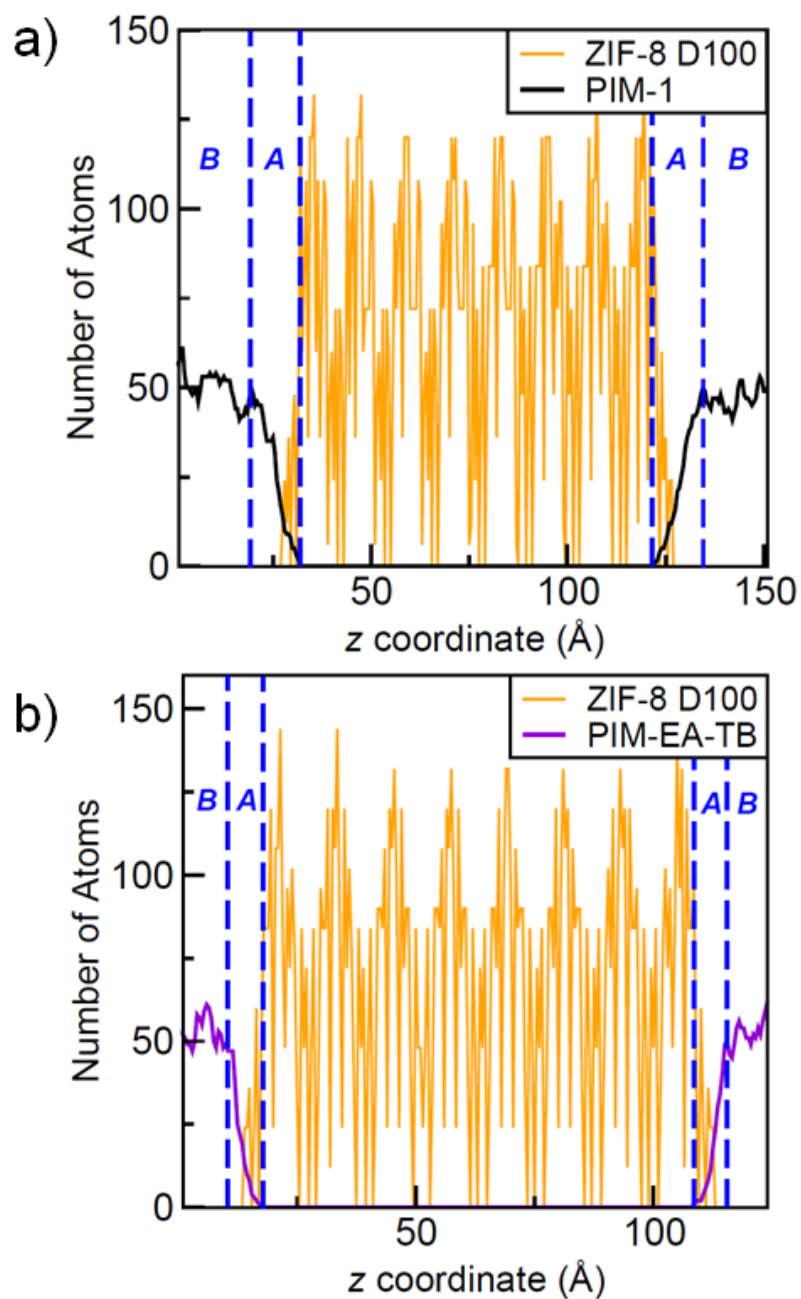


Fig. 4. Densities of polymer and MOF atoms as a function of the z coordinate for representative configurations of: (a) ZIF-8(D1)/PIM-1 and (b) ZIF-8(D1)/PIM-EA-TB. The blue dashed lines indicate the limits of **region A** and **B**.

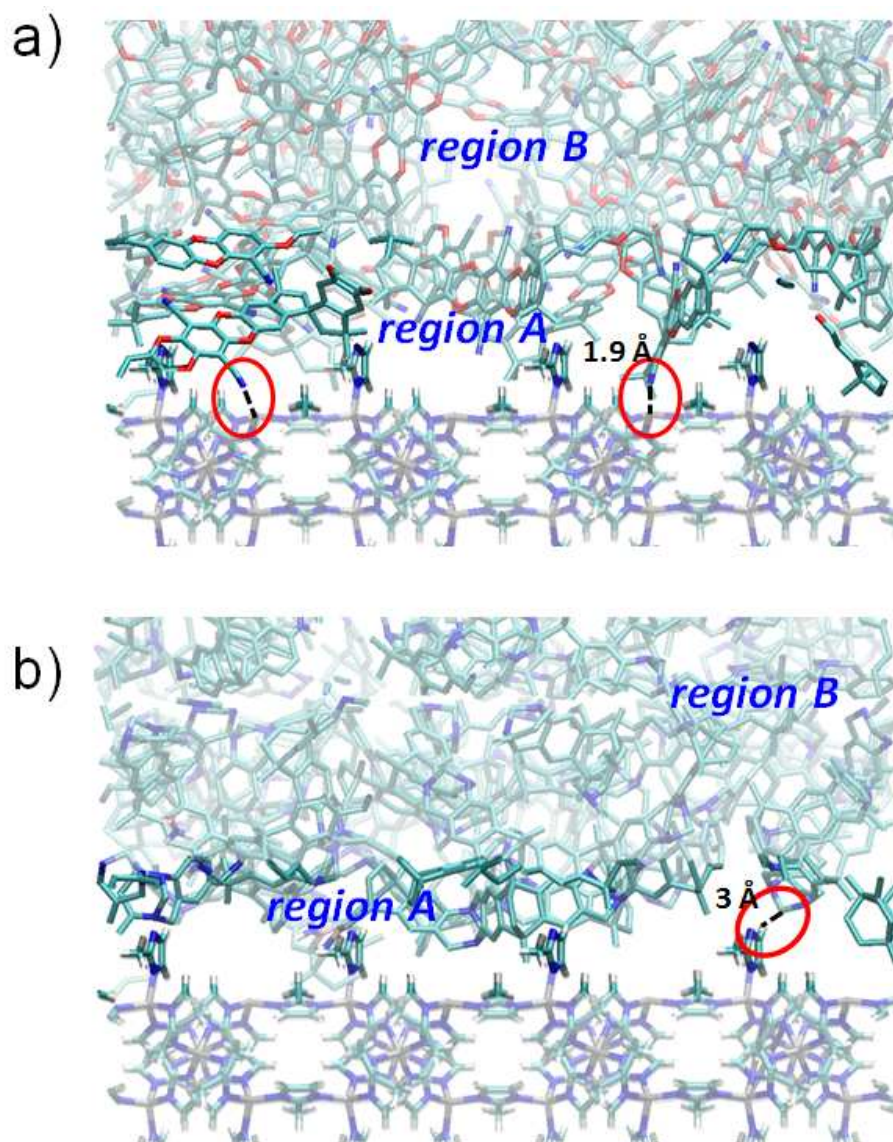


Fig 5. Illustrations of the modeled MOF/polymer interfaces. (a) ZIF-8(D1)/PIM-1, typical $(\text{Zn})_{\text{ZIF-8}} \dots \text{CN}_{\text{PIM-1}}$ interactions are circled in red. (b) ZIF-8(D1)/PIM-EA-TB, a typical $(\text{H})_{\text{ZIF-8}} \dots \text{CH}_{\text{PIM-EA-TB}}$ interaction is circled in red.

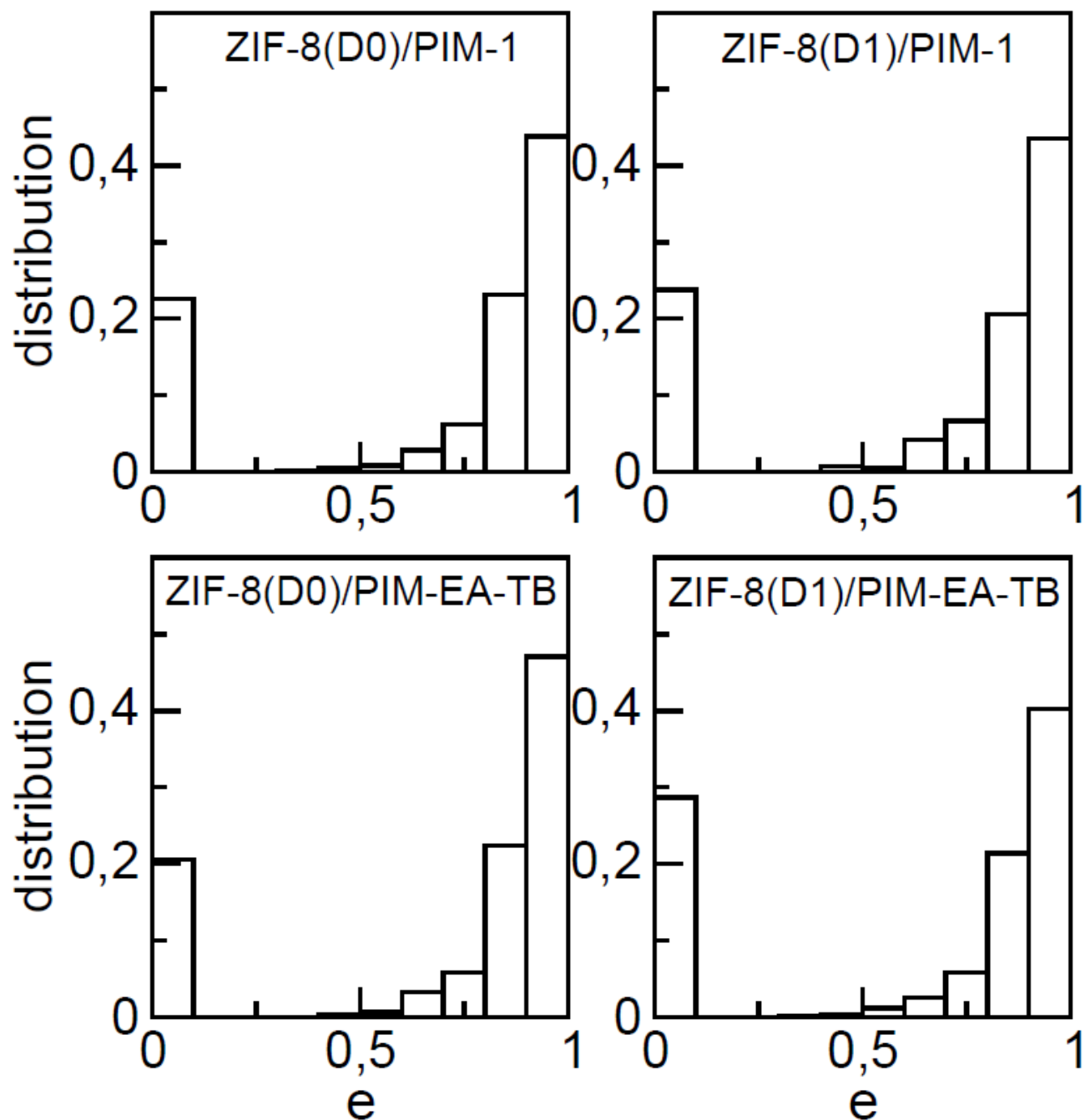


Fig. 6. Eccentricity of the microvoids in **region A** for the ZIF-8/PIM-1 and ZIF-8/PIM-EA-TB “defect-free” (D0) and “defect-containing” (D1) interfaces.

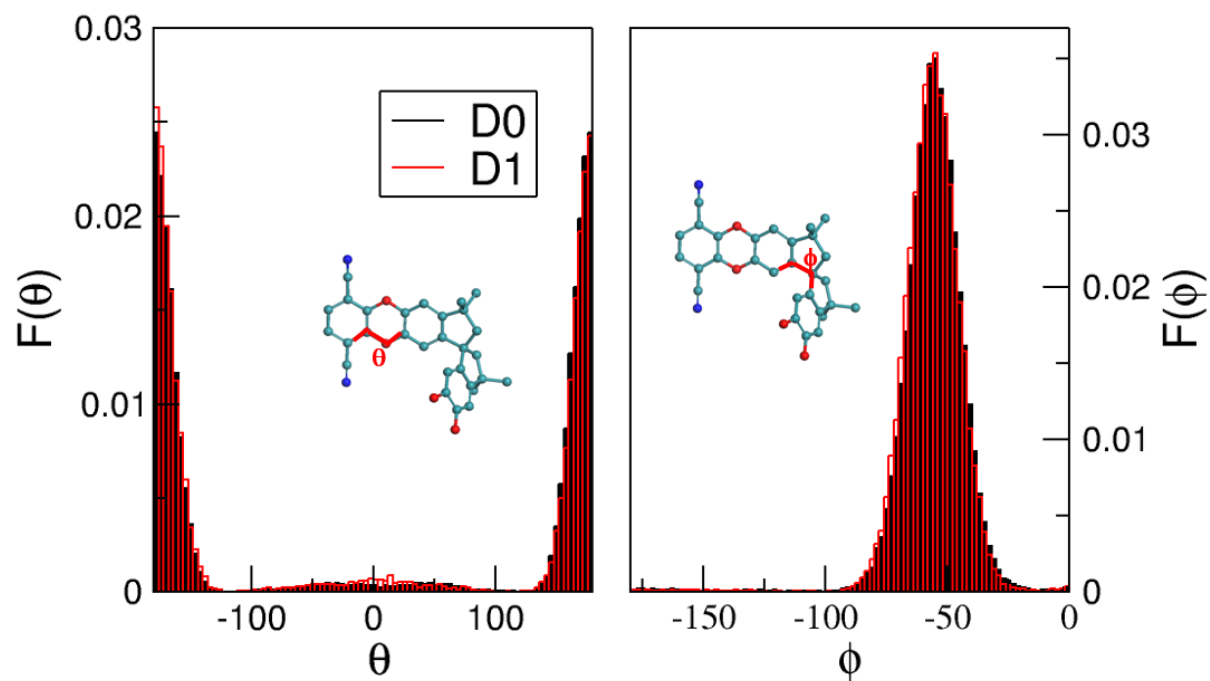


Fig. 7. Dihedrals angles distributions for the polymer phase in ZIF-8(D1)/PIM-1 (black full histogram) and ZIF-8(D1)/PIM-1 (red empty histogram).

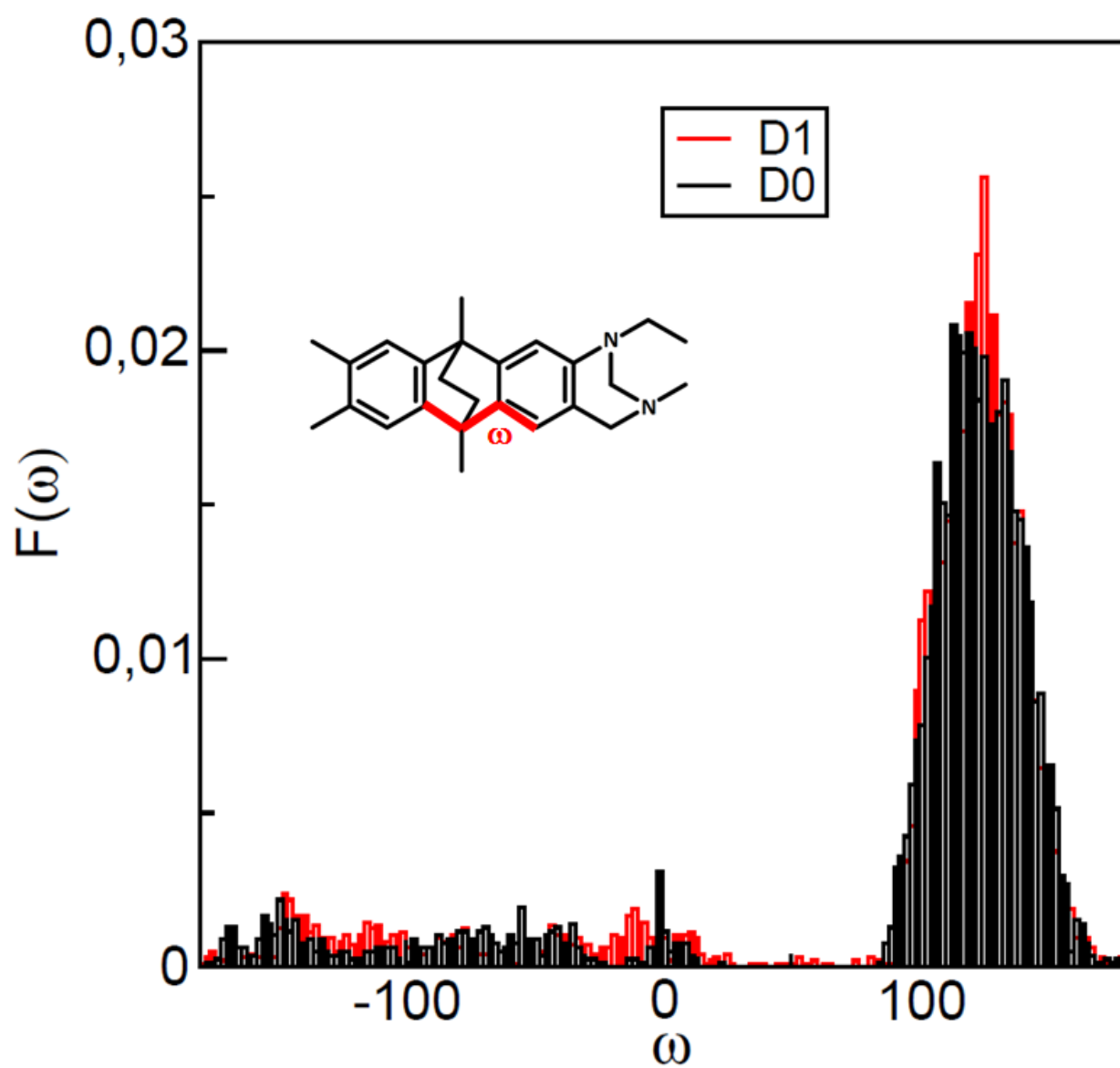


Fig 8. Dihedral angle distribution for the polymer phase in ZIF-8(D0)/PIM-EA-TB (black) and ZIF-8(D1)/PIM-EA-TB (red).

Comprehension of the compatibility and thus stability between a MOF and a polymer in the presence of defects at the MOF surface

ACCEPTED MANUSCRIPT